Supporting Information

GaSb Doping Facilitates Conduction Band Convergence and Improves Thermoelectric Performance in n-type PbS

Zixuan Chen,[1,2,12] Hong-Hua Cui,[3,12] Shiqiang Hao,[4] Yukun Liu,[4] Hui Liu,[5] Jing Zhou,[1] Yan Yu,[1,2,6] Qingyu Yan,[7,8] Christopher Wolverton,[4] Vinayak P. Dravid,[4] Zhong-Zhen Luo,[1,2,6,*] Zhigang Zou,[1,2,9,10] Mercouri G. Kanatzidis[11,*]

[1]Key Laboratory of Eco-materials Advanced Technology, College of Materials Science and Engineering, Fuzhou University, Fuzhou, 350108, China

[2]Fujian Science & Technology Innovation Laboratory for Optoelectronic Information of China, Fuzhou, Fujian 350108, China

[3]Mechanical and Electrical Engineering Practice Center, Fuzhou University, Fuzhou, 350108, China

[4]Department of Materials Science and Engineering, Northwestern University, Evanston, Illinois 60208, United States

[5]Beijing Advanced Innovation Center for Materials Genome Engineering, University of Science and Technology Beijing, Beijing 100083, China

[6]Key Laboratory of Advanced Materials Technologies, International (HongKong Macao and Taiwan) Joint Laboratory on Advanced Materials Technologies, College of Materials Science and Engineering, Fuzhou University, Fuzhou, Fujian, 350108, China

[7]School of Materials Science and Engineering, Nanyang Technological University, 50 Nanyang Avenue 639798, Singapore

[8]Institute of Materials Research and Engineering, A*STAR, 138634, Singapore

[9]Eco-materials and Renewable Energy Research Center, College of Engineering and Applied Sciences, Nanjing University, Nanjing, 210093, China

[10]National Laboratory of Solid State Microstructures, Nanjing University, Nanjing 210093, China.

[11]Department of Chemistry, Northwestern University, Evanston, Illinois 60208, United States

[12]These authors contributed equally: Zixuan Chen, Hong-Hua Cui

Corresponding authors: E-mail: zzluo@fzu.edu.cn (Z. Z. Luo),

E-mail: m-kanatzidis@northwestern.edu (M. G. Kanatzidis)

Synthesis. The high-purity elements were used as obtained: Pb wire (4N, American Elements, USA), Ga shots (4N, Sigma-Aldrich, USA), Sb shots (5N, American Elements, USA), and S flakes (5N, American Elements, USA). The GaSb semiconductor was synthesized by the stoichiometric ratio of Ga and Sb shots under 1023 K, dwelt for 12 h in an evacuated quartz tube. All samples with a predetermined nominal stoichiometric ratio of $Pb_{1-x}(GaSb)_xS$ (x = 0, 0.1%, 0.3%, 0.6%, and 0.9%), $Pb_{1-x}Ga_xS$ (x = 0, 0.1%, 0.3%, 0.5%, and 0.7%) and $Pb_{1-x}Sb_xS$ (x = 0, 0.1%, 0.3%, 0.5%, and 0.7%) were synthesized by a facile melting-quenching process. The tubes containing the raw materials were flame-sealed at a pressure of approximately 2×10^{-3} torr. The sealed tubes were then slowly heated to 723 K over a period of 12 hours. After this, the tubes were heated to 1423 K in 7 hours, soaked at this temperature for 6 hours, and periodically shaken in a box furnace. Finally, the tubes were air quenched to room temperature. The same method was used to prepare Ga- or Sb-doped PbS samples for lattice parameter measurement. For a typical sample, the following amounts of raw materials were used: Pb (10 g, 48.263 mmol), GaSb (0.0278 g, 0.145 mmol), and S (1.5522 g, 48.408 mmol) for preparing a ~11.6 g ingot sample of $Pb_{0.997}(GaSb)_{0.003}S$.

Densification. The ingots were ground to fine powders using a mortar and pestle. The powder samples were loaded into a 12.7 mm graphite die and sintered using the Spark Plasma Sintering (SPS) technique (SPS-211LX, Fuji Electronic Industrial Co. Ltd., Japan) at 773 K for 5 min under a constant axial pressure of 40 MPa. The relative density above 96% of the pellets was obtained. The grain size of the pellets is almost distributed between 0-5 μm^2 (Figure S5, Supporting information).

Powder X-ray Diffraction (PXRD) Characterization. The PXRD patterns of SPSed samples were performed for purity analysis using a Rigaku Miniflex powder X-ray diffractometer with Ni-filtered Cu K_α (λ = 1.5418 Å) radiation operating at 40 kV and 15 mA.

Scanning/Transmission Electron Microscopy (S/TEM) Characterization. To confirm the phase nature of the $Pb_{1-x}(GaSb)_xS$ compounds, scanning electron microscopy (SEM) analyses were applied with a Schottky field emission SEM (JEOL

JSM-7900FLV SEM) under 15 kV. Scanning/transmission electron microscopy (S/TEM) and STEM energy dispersive spectroscopy (EDS) experiments were carried out using a JEOL ARM300F microscope and an aberration-corrected JEOL ARM200CF operated at 300 kV and 200 kV, respectively. The TEM specimens were prepared by conventional methods, including cutting, grinding, and Ar-ion milling (4.5 kV for ~0.5 h until a hole is formed, followed by ion cleaning with 0.3 kV for 40 minutes) under low temperature (liquid nitrogen stage).

Electron backscattered diffraction (EBSD) Sample Preparation and Charaterization. The cut samples were cold-mounted into quick-dry epoxy, with the large face exposed. The sample was then ground using 600 and 800 grit SiC grinding paper for 3 minutes and followed with 1200 grit SiC grinding paper for 10 minutes. Next, samples were polished for 30 min and 45 min with 1 μm glycol-based diamond slurry and 0.05 μm colloidal silica suspension, respectively. Upon finishing this step, samples were placed into a vibratory polisher for 3 h at 62.7 Hz in a bath of 0.05 μm colloidal silica suspension. The samples were then ion milled at 5 kV accelerating voltage and 1.5 kV discharge voltage to remove the deformation layer caused by grinding and polishing. For EBSD analysis, accelerating voltage was set to 30 kV with a working distance of approximately 10 mm and was carried out using a FEI Quanta 650 ESEM. EBSD patterns were collected over an area of 80 μm × 50 μm with a 0.2 μm step size using an Oxford Aztec EBSD system.

Electronic Transport Properties. The electrical conductivity σ and Seebeck coefficient S of SPSed samples were simultaneously measured using a ZEM-3 system (Ulvac Riko, Japan). The bar-shaped samples cut from SPSed pellets with ~12 mm × 4 mm × 4 mm coated with boron nitride were measured from 300 K to 923 K under a low-pressure Helium atmosphere. We added a thin layer of graphite paper to increase the contact on the top and bottom of the test electrodes.

Hall Measurements. Hall coefficient (R_H) was measured with a Xiangjin self-made Hall electrical performance test system (NYMS) under a helium atmosphere. The square samples of ~9 × 9 × 1 mm^3 were cut and polished from the disks. The four electrodes arranged in a van der Pauw configuration were mechanically pressed to

contact the edges of the square sample. The R_H was measured using the van der Pauw technique under a reversible magnetic field of 1.5 T, each involving five measurements. The carrier concentration n was estimated from the R_H with the relationship $n = 1/(e|R_H|)$, in which e is the electron charge.

Thermal Conductivity. The thermal diffusivity, D was measured using the laser flash diffusivity method (LFA 467 MicroFlash, NETZSCH, Germany) and analyzed using a Cowan model with pulse correction. The square-shaped pellets with dimensions of ~10 × 10 × 2 mm^3 coated with a thin layer of graphite were used for the measurement under a continuous nitrogen flow from 300 K to 923 K. The κ_{tot} was calculated with the relationship $\kappa_{tot} = D\rho C_p$, where ρ and C_p are density and specific heat capacity, respectively. The C_p was determined by the relation of C_p/k_B per atom = $3.07 + 4.7 \times 10^{-4} \times (T - 300)$.[1-3] The ρ was calculated using the sample's dimension and mass.

Band Structure Calculations. The Density Functional Theory (DFT) was utilized to calculate the relaxed geometries of various dopants in PbS host and corresponding total energies within the generalized gradient approximation of Perdew-Burke-Ernzerhof the exchange-correlation functional with Projector Augmented Wave potentials.[4] The periodic boundary conditions and a plane wave basis set are applied as implemented in the Vienna *ab initio* simulation package.[5] The basis set energy cutoff of 500 eV and total energy numerically convergence criterion of approximately 3 meV/cation were adopted in all relaxation calculations. For the k-point parameter, we used dense k-meshes corresponding to 4000 k-points per reciprocal atom in the Brillouin zone. For the band structure calculations, spin-orbit coupling is applied. It needs to mention that for the Ga and Sb co-doped sample, we first evaluate many possible configurations of one Ga atom and one Sb atom substitution sites and perform the band structure calculation for the energetically most favorable one. In detail, there are several configurations for Ga and Sb substitution for one Pb atom in the 54 atom PbS host lattice. We found that both Ga and Sb strongly prefer the cation substitution of Pb over the anion substitution of S. Specifically, the Ga substitution of Pb is more favorable than the substitution of S by 2.49 eV/Ga. Similarly, the Sb substitution of Pb is also more favorable than that of S by 0.79 eV/Sb. We considered a Ga substitution for Pb

and an interstitial Sb located in the first, second, and third nearest neighbor to the Ga atom. Similarly, an Sb substitution for Pb with a Ga interstitial as the first, second, and third nearest neighbors. We found that the configuration with Ga and Sb residing as the first nearest neighbor with the mass center of Ga-Sb in the normal Pb site is energetically more favorable than others. We then performed the band structure calculations based on this most favorable substitution.

DFT for phonon dispersion calculations. The dynamical properties of relaxed structures are calculated by the frozen-phonon method.[6, 7] In this method, the force-constant matrix is constructed from *ab-initio* forces exerted on all cell atoms when a particular cell atom is slightly displaced from its equilibrium position. The DFT calculations were carried out using the VASP[8] code with GGA-PBE[4] for the electronic exchange-correlation functional. The vibration phonon modes were obtained from the diagonalization from the corresponding dynamical matrix. This method has recently been shown to produce accurate values of κ_{lat}, compared to experiments, for low thermal conductivity thermoelectric compounds.[9-11]

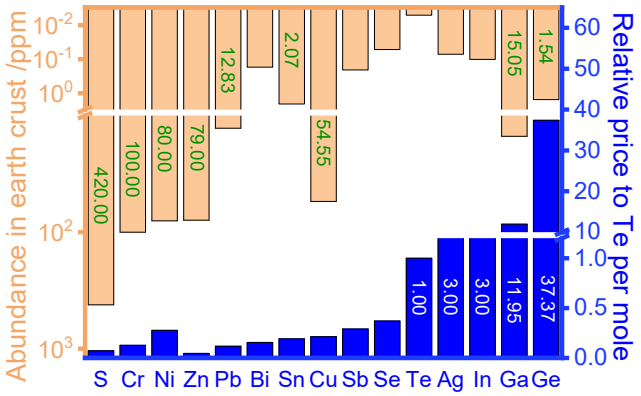

Figure S1. The abundance of various elements employed in thermoelectric materials in the Earth's crust and the price of elements compared with that Te from the Alfa Aesar Co. website.

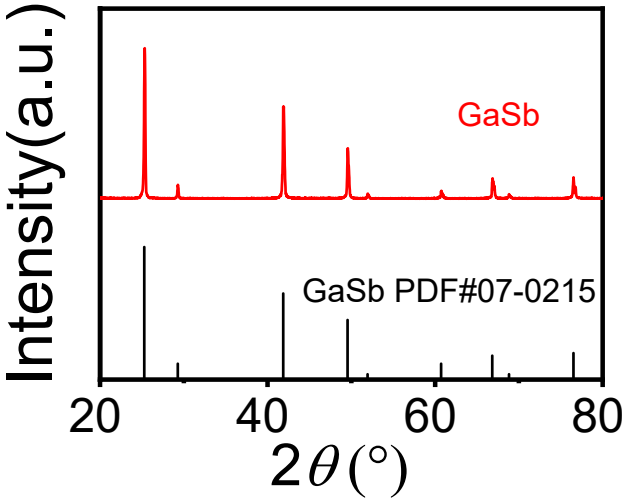

Figure S2. PXRD patterns of GaSb with all peaks indexed by the referenced patterns JCPDS 78−1055.

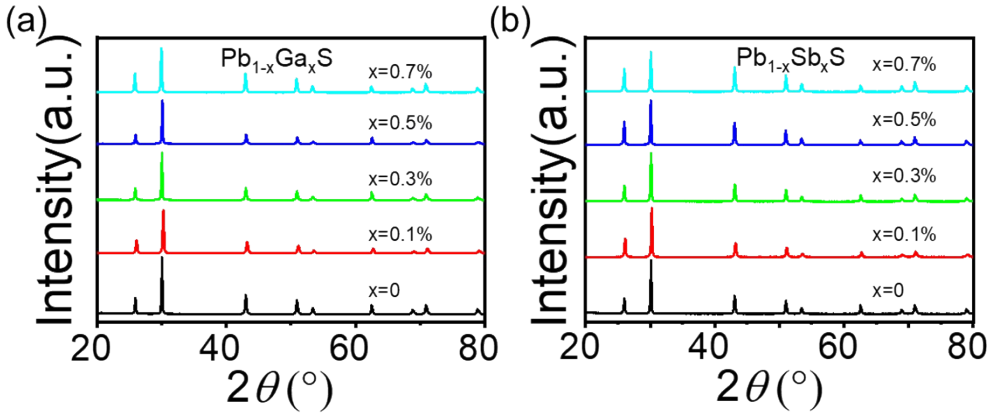

Figure S3. PXRD patterns of (a) $Pb_{1-x}Ga_xS$ and (b) $Pb_{1-x}Sb_xS$ (x = 0, 0.1%, 0.3%, 0.5%, and 0.7%).

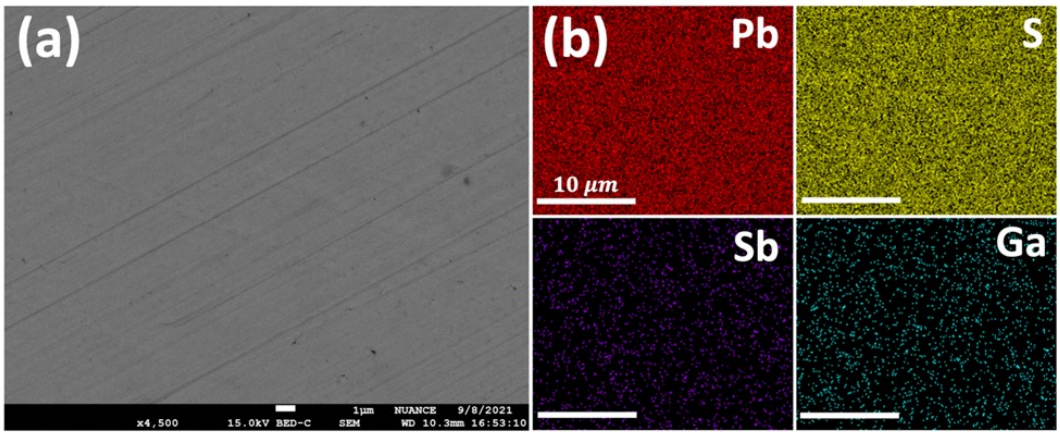

Figure S4. Microstructure and composition analysis of the $Pb_{0.997}(GaSb)_{0.003}S$ sample. (a) Back-scattered SEM (BSE) image of the specimen. (b) EDS mapping of the region is shown in (a).

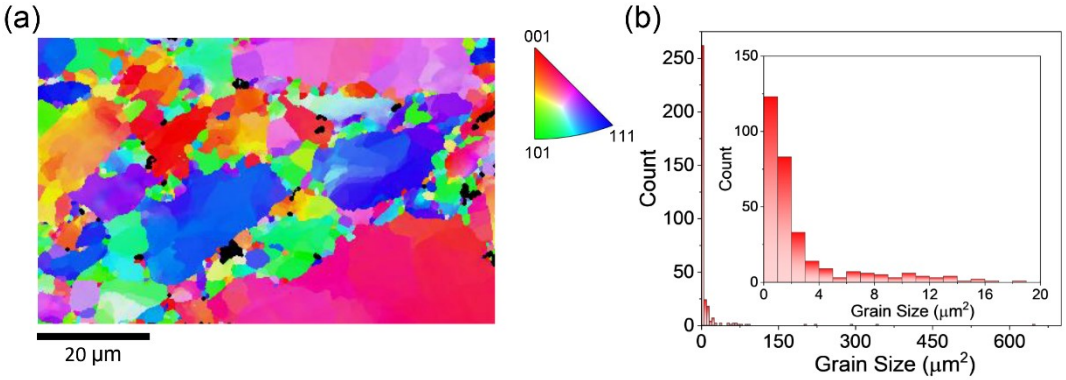

Figure S5. Grain size analysis of the $Pb_{0.997}(GaSb)_{0.003}S$ sample. (a) Electron backscattered diffraction (EBSD) image of the specimen and (b) The grain size distribution of the specimen.

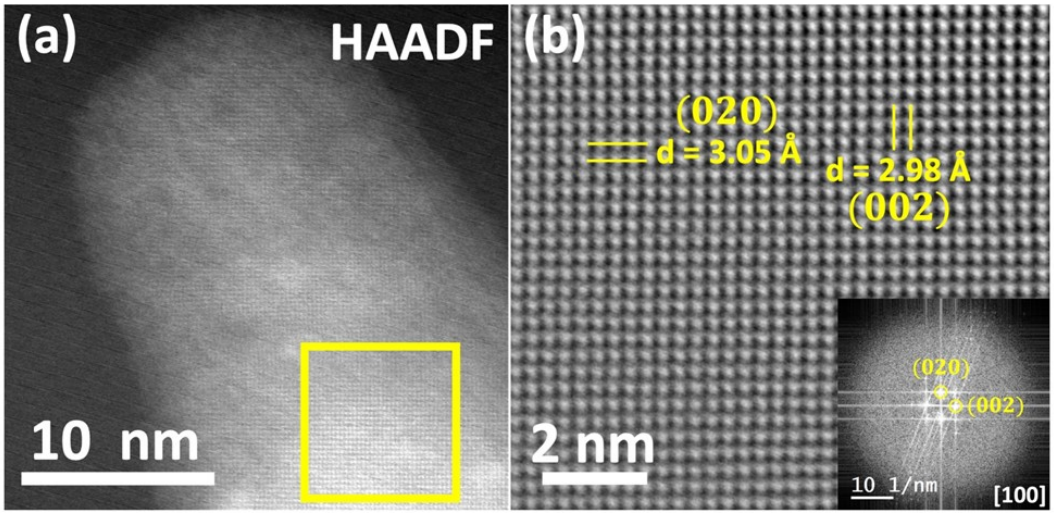

Figure S6. STEM analysis of the $Pb_{0.997}(GaSb)_{0.003}S$ sample. (a) HAADF image of the specimen along the [100] zone axis. (b) Atomic-resolution HAADF-STEM image of the region surrounded by the yellow box in (a) with atomic plane spacings labeled. The inset is the fast Fourier transform (FFT) of the image with atomic planes labeled.

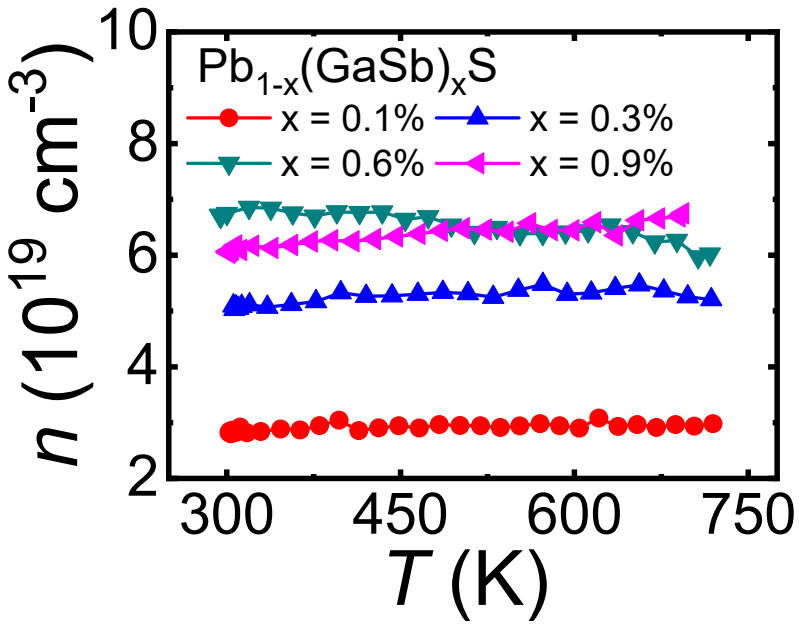

Figure S7. Temperature-dependent carrier concentration, *n* for $Pb_{1-x}(GaSb)_xS$ (x = 0.1%, 0.3%, 0.6%, and 0.9%) samples.

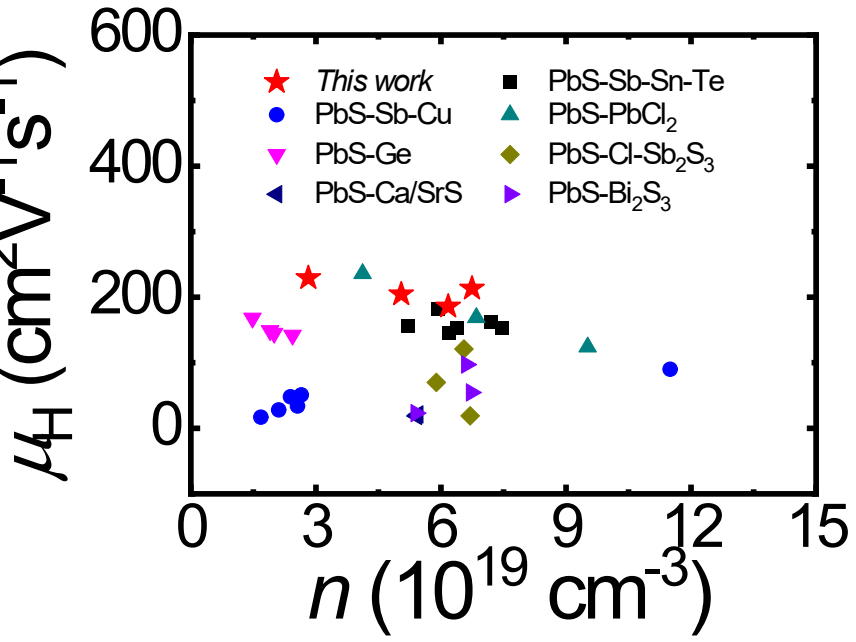

Figure S8. Comparison of carrier mobility, μ_H in this work ($Pb_{1-x}(GaSb)_xS$) with previous n-type PbS-based sample, $Pb_{0.93}Sb_{0.01}Sn_{0.06}S$-x%PbTe (PbS-Sb-Sn-Te),[12] $Pb_{0.98-x}Sb_{0.02}Cu_xS$-yCu (PbS-Sb-Cu),[13] PbS-x$PbCl_2$ (PbS-Cl),[14] PbS-1%$PbCl_2$-xSb_2S_3 (PbS-Cl-Sb_2S_3),[14] PbS-1%$PbCl_2$-1%Ca/SrS (PbS-Ca/SrS),[14] $Pb_{1-x}Ge_xS$,[15] and PbS-1%$PbCl_2$-xBi_2S_3 (PbS-Bi_2S_3).[14]

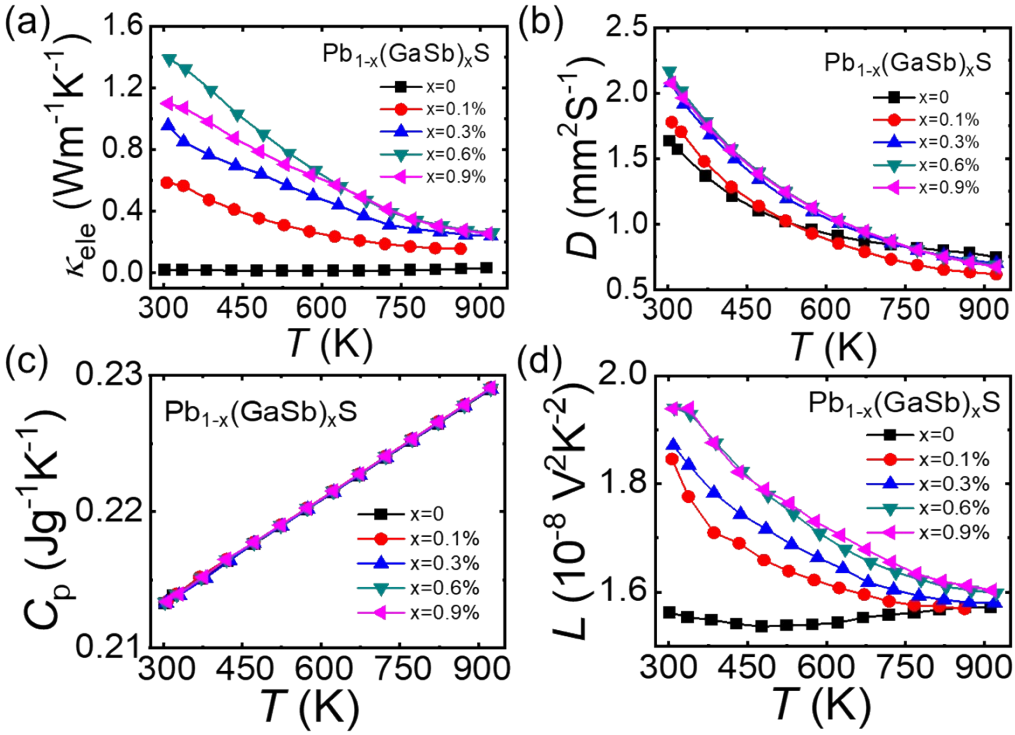

Figure S9. Temperature-dependent (a) electronic thermal conductivity, κ_{ele}; (b) thermal diffusivity, D; (c) heat capacity, C_p; and (d) Lorenz numbers, L for $Pb_{1-x}(GaSb)_xS$ samples.

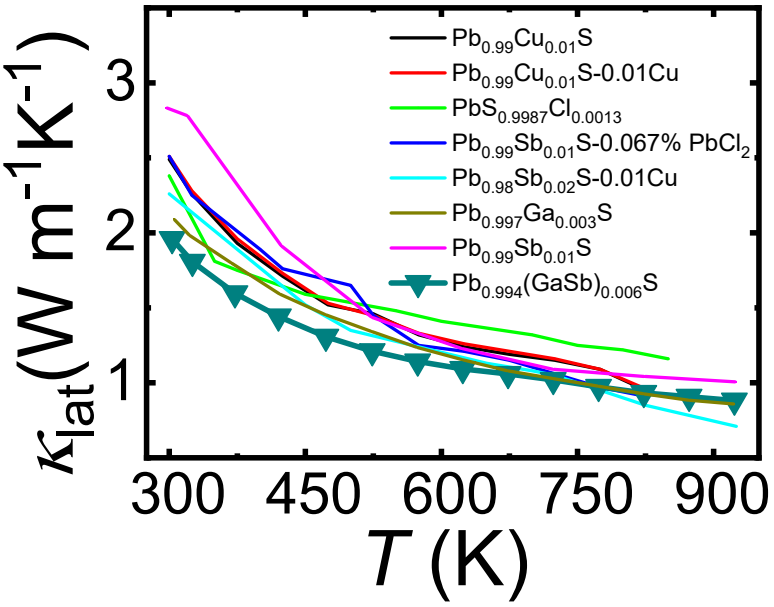

Figure S10. Comparison of κ_{lat} values for PbS-based thermoelectric materials: $Pb_{0.99}Cu_{0.01}S$,[16] $Pb_{0.99}Cu_{0.01}S$-0.01Cu,[16] $PbS_{0.9987}Cl_{0.0013}$,[17] $Pb_{0.99}Bi_{0.01}S$-0.067%$PbCl_2$,[18] $Pb_{0.98}Sb_{0.02}S$-0.01Cu,[13] $Pb_{0.997}Ga_{0.003}S$,[19] and $Pb_{0.99}Sb_{0.01}S$[20] with relatively low alloying content.

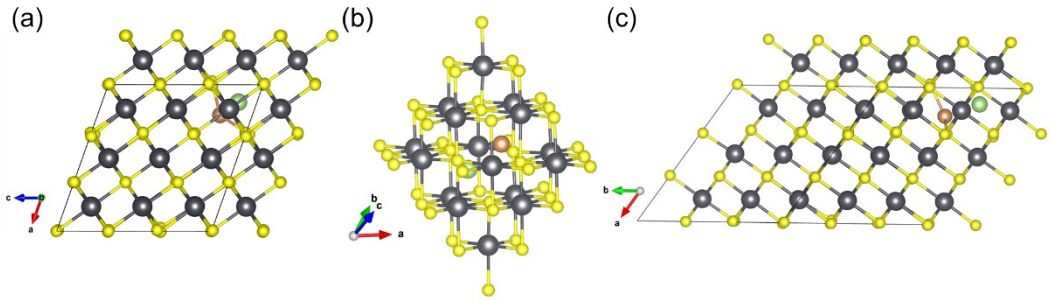

Figure S11. The calculated crystal structure of the GaSb-doped PbS with different directions: (a) *b* axis, (b) near <111> direction, and (c) *c* axis.

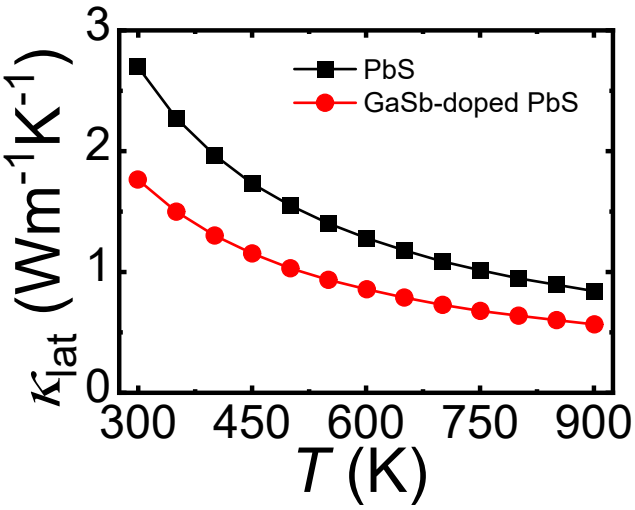

Figure S12. Comparison of the κ_{lat} as a function of temperature for pure PbS and GaSb-doped PbS, calculated from the DFT phonon dispersion curves and Debye–Callaway formalism.

Table S1. The DOS effective masses for pure PbS, Ga-doped PbS, Sb-doped PbS, and GaSb-doped PbS samples.

Composition	m^* (m_e)
PbS	0.46
Ga-doped PbS	0.52
Sb-doped PbS	0.54
GaSb-doped PbS	0.64

Table S2. Room temperature mass densities for $Pb_{1-x}(GaSb)_xS$ (x = 0, 0.1%, 0.3%, 0.6%, and 0.9%) samples.

Composition	Measured density, gcm^{-3}	Theoretical density, %
PbS	7.31	96.2
$Pb_{0.999}(GaSb)_{0.001}S$	7.29	96.8
$Pb_{0.997}(GaSb)_{0.003}S$	7.26	96.4
$Pb_{0.994}(GaSb)_{0.006}S$	7.26	96.5
$Pb_{0.991}(GaSb)_{0.009}S$	7.31	97.1

References

1. K. Yamaguchi, K. Kameda, Y. Takeda and K. Itagaki, *Mater. Trans. JIM*, 1994, **35**, 118-124.
2. A. S. Pashinkin, M. S. Mikhailova, A. S. Malkova and V. A. Fedorov, *Inorg. Mater.*, 2009, **45**, 1226.
3. R. Blachnik and R. Igel, *Journal*, 1974, **29**, 625.
4. J. P. Perdew, K. Burke and M. Ernzerhof, *Phys. Rev. Lett.*, 1996, **77**, 3865.
5. G. Kresse and J. Furthmüller, *Phys. Rev. B*, 1996, **54**, 11169-11186.
6. K. Parlinski, Z. Q. Li and Y. Kawazoe, *Phys. Rev. Lett.*, 1997, **78**, 4063-4066.
7. L. Chaput, A. Togo, I. Tanaka and G. Hug, *Phys. Rev. B*, 2011, **84**, 094302.
8. G. Kresse and D. Joubert, *Phys. Rev. B*, 1999, **59**, 1758-1775.
9. M. Asen-Palmer, K. Bartkowski, E. Gmelin, M. Cardona, A. P. Zhernov, A. V. Inyushkin, A. Taldenkov, V. I. Ozhogin, K. M. Itoh and E. E. Haller, *Phys. Rev. B*, 1997, **56**, 9431-9447.
10. Y. Zhang, E. Skoug, J. Cain, V. Ozoliņš, D. Morelli and C. Wolverton, *Phys. Rev. B*, 2012, **85**, 054306.
11. D. T. Morelli, J. P. Heremans and G. A. Slack, *Phys. Rev. B*, 2002, **66**, 195304.
12. Y. Xiao, D. Y. Wang, Y. Zhang, C. R. Chen, S. X. Zhang, K. D. Wang, G. T. Wang, S. J. Pennycook, G. J. Snyder, H. J. Wu and L. D. Zhao, *J. Am. Chem. Soc.*, 2020, **142**, 4051-4060.
13. M. Zhao, C. Chang, Y. Xiao, R. Gu, J. He and L.-D. Zhao, *J. Alloys Compd.*, 2018, **781**, 820-830.
14. L. D. Zhao, S. H. Lo, J. Q. He, H. Li, K. Biswas, J. Androulakis, C. I. Wu, T. P. Hogan, D. Y. Chung, V. P. Dravid and M. G. Kanatzidis, *J. Am. Chem. Soc.*, 2011, **133**, 20476-20487.
15. E. Rathore, R. Juneja, D. Sarkar, S. Roychowdhury, M. Kofu, K. Nakajima, A. K. Singh and K. Biswas, *Mater. Today Energy*, 2022, **24**, 100953.
16. Y. Qin, T. Hong, B. Qin, D. Wang, W. He, X. Gao, Y. Xiao and L.-D. Zhao, *Adv. Funct. Mater.*, 2021, **31**, 2102185.
17. H. Wang, E. Schechtel, Y. Pei and G. J. Snyder, *Adv. Energy Mater.*, 2013, **3**, 488-495.
18. J. Yang, X. Zhang, G. Liu, L. Zhao, J. Liu, Z. Shi, J. Ding and G. Qiao, *Nano Energy*, 2020, **74**, 104826.
19. Z.-Z. Luo, S. Hao, S. Cai, T. P. Bailey, G. Tan, Y. Luo, I. Spanopoulos, C. Uher, C. Wolverton, V. P. Dravid, Q. Yan and M. G. Kanatzidis, *J. Am. Chem. Soc.*, 2019, **141**, 6403-6412.
20. M. Zhao, C. Chang, Y. Xiao and L.-D. Zhao, *J. Alloys Compd.*, 2018, **744**, 769-777.